Pore-Size Evaluation and Gas Transport Behaviors of Microporous Membranes: An Experimental and Theoretical Study

Gang Li
Department of Light Chemical Engineering, School of Light Industry & Food Science, South China University of Technology, Guangzhou 510641, China

Hye Ryeon Lee
Research Center for Green Fine Chemicals, Korea Research Institute of Chemical Technology, UIsan 681–802, Republic of Korea

Hiroki Nagasawa, Masakoto Kanezashi, Tomohisa Yoshioka, and Toshinori Tsuru
Dept. of Chemical Engineering, Hiroshima University, Higashi-Hiroshima 739–8527, Japan

DOI 10.1002/aic.14812
Published online April 13, 2015 in Wiley Online Library (wileyonlinelibrary.com)

A modified gas-translation (GT) model based on a GT mechanism was successfully applied to the pore-size evaluation and gas transport behavior analysis of microporous membranes with different pore-size distributions. Based on the gas permeation results of three microporous membranes derived from different alkoxides, the effects of activation energy and the selection of a standard gas on the pore-size evaluation were discussed in a comparative study. The presence of nano-sized defects had an important influence on the gas permeation performance of microporous membranes, depending largely on the original pore size of the membrane in question. Moreover, the gas-separation effect of the pore-size distribution in a silica membrane was theoretically studied and revealed a significant increase in gas permeance for relatively large gas species but not for small ones. © 2015 American Institute of Chemical Engineers *AIChE J*, 61: 2268–2279, 2015
Keywords: membrane separation, pore-size evaluation, gas transport behavior, modified gas-translation model, normalized Knudsen-based permeance

Introduction

Microporous inorganic membranes have attracted significant interest for molecular separation in both gas and liquid mixtures, because of their excellent hydrothermal stability and high separation efficiency. The pore size of a microporous membrane plays a significant role in determining membrane performance in various processes. Thus, the characterization of the membrane pore size is of great importance for membrane development and applications. Although a variety of effective methods have been developed to characterize the pore sizes of powdered porous materials, only a few techniques are presently available to evaluate the pore sizes of microporous membranes. A well-known technique that is used to measure the pore size of a membrane is permporometry.[1–3] This method measures the permeance of a noncondensable gas as a function of the activity of condensable gas that can block noncondensable gas permeation due to the capillary condensation effect. Using the Kelvin equation, these gas permeation data can then be correlated with the pore sizes of membranes. When using this method, however, reliable characterization generally requires membrane pore sizes that range from 1 to 50 nm.[4] For an evaluation of a pore-size distribution that is smaller than 1 nm, the commonly used method is to measure the single-gas permeation through the membrane at a high temperature with a series of probe gases with different kinetic diameters. Judging from the gas permeation cutoff against the molecular size of permeating gases, a possible range for the pore size of a microporous membrane can be roughly determined.

For a quantitative evaluation of the pore size of microporous membranes in the subnano range, Lee et al.[5] recently proposed a simple and effective normalized Knudsen-based permeance (NKP) method by modifying a GT model that was developed by Xiao and Wei[6] and Shelekhin et al.[7] In this method, NKP is defined as the ratio of experimentally obtained gas permeance at a high temperature to the predicted gas permeance under a Knudsen diffusion mechanism based on a standard gas. When a membrane is assumed to consist of uniform cylindrical pores, and the difference in the activation energy for gas permeation can reasonably be ignored, NKP can be correlated with the gas kinetic diameter and membrane pore size under a constant temperature. Therefore, the pore size of a microporous membrane can be obtained by fitting a set of NKP against the kinetic diameter of the permeating gases. However, when the activation

Correspondence concerning this article should be addressed to T. Tsuru at tsuru@hiroshima-u.ac.jp

© 2015 American Institute of Chemical Engineers

energy of gas permeation is relatively high, its effect on gas permeation will be substantial, and, therefore, the NKP must be modified in the NKP plot to ensure its accuracy. Yoshioka et al.[4] modified the NKP by considering the contribution of the effect of activation energy on gas permeation, and showed improved estimation of the pore sizes of microporous membranes. Previous studies have shown that the NKP method is a reliable pore-size characterization technique, and has been successfully applied to a variety of zeolite and silica membranes.[4,5,8–10] However, for membranes with typical bimodal or multimodal pore structures, these current equations for correlating NKP with the membrane pore size are not applicable and must be modified because of the different pore structures.

In this study, three silica membranes were fabricated using different alkoxides to further examine the validity of applying the modified GT model to the pore-size evaluation of microporous membranes. The effects of the activation energy of gas permeation and the selection of a standard gas on pore-size determination were discussed in the NKP method. Moreover, based on the modified GT model, theoretical analysis of the effect of membrane pore size on gas-separation performance was performed. For membranes with bimodal and multimodal pore structures, new equations were formulated to correlate NKP with the membrane pore size, and these were then used to theoretically study the effect of defects and pore-size distribution on gas transport behaviors.

Theory

Gas transport through porous membranes can occur in various mechanisms, depending on the membrane structure, operating conditions, and the properties of the permeating molecules. For microporous membranes with a pore size <2 nm, the pore diameter is usually smaller than the mean free path of the permeating gas molecules, and therefore, the gas molecules collide much more frequently with the pore wall than with each other. The collisions between the molecules themselves can be thought of as negligible. Gas permeation through membranes in this manner is known as Knudsen diffusion, and the gas permeance through a membrane by this mechanism can be expressed as follows

$$P_{K,i}=\frac{\varepsilon d_e}{3\tau L}\sqrt{\frac{8}{\pi M_i RT}} \tag{1}$$

In the ideal Knudsen diffusion, the effect of the interaction between the diffusing gas and the pore wall is not involved during membrane permeation. However, when the pore size is small enough, the diffusion barrier imposed by the pore wall becomes obvious. For this reason, a GT mechanism (called the activated Knudsen diffusion mechanism) has been proposed for non-adsorptive or weak-adsorptive gas diffusion in micropores. It should be noted that, when the gas is adsorptive, to ensure its diffusion still in the GT region, the presence of surface flow in the pores must be avoided, and a relatively high permeation temperature generally can be used to satisfy this purpose.

Gas permeance through a microporous membrane under a GT mechanism can be expressed as follows[6,7]

$$P_{GT,i}=\frac{\varepsilon d_e \rho_i}{\tau L}\sqrt{\frac{8}{\pi M_i RT}} \tag{2}$$

where the diffusion probability for component i, ρ_i, is described with a pre-exponential factor, $\rho_{g,i}$, and with the kinetic energy, $E_{p,i}$, that is required to overcome the diffusion barrier, as shown in Eq. 3

$$\rho_i=\rho_{g,i}\exp\left(-\frac{E_{p,i}}{RT}\right) \tag{3}$$

$\rho_{g,i}$ is given by the product of the following terms:[5] (1) the ratio of the effective cross-sectional area of a pore for the i-th component, $A_{e,i}$, to the physical cross-sectional pore area of the pore, A_0, and (2) the random factor 1/3 in a three-dimensional space, as shown in Eq. 4

$$\rho_{g,i}=\frac{1}{3}\frac{A_{e,i}}{A_0} \tag{4}$$

The porosity of a membrane, ε, is defined by the ratio of the pore area on the membrane to the total membrane area. When the membrane is assumed to have uniform cylindrical pores, the porosity of the membrane, ε, can be further expressed as follows

$$\varepsilon=\frac{A_0}{A_m}=\frac{\pi {d_p}^2 N_p}{4A_m} \tag{5}$$

After substituting $\rho_{g,i}$, and ε from Eqs. 4 and 5 into Eq. 2, and when the pore diameter, d_p, is taken as the effective diffusion length, the GT model can be further denoted as follows

$$P_{GT,i}=\frac{N_p {d_p}^3}{6\tau L A_m}\sqrt{\frac{2\pi}{M_i RT}}\exp\left(-\frac{E_{p,i}}{RT}\right) \tag{6}$$

It should be noted that the effective diffusion length is not equivalent to the pore size of the membrane if the pore size is very small (e.g., <1 nm), because the effect of the actual size of gas molecules on the diffusion length must be taken into consideration under this circumstance. Therefore, when the difference in the gas molecular size and the pore diameter is quite small, the effective diffusion length, d_e, must be expressed as $d_{e,i}$ by Eq. 7 [4,5]

$$d_{e,i}=d_p-d_{k,i} \tag{7}$$

Thus, the ratio of the effective diffusion area, A_e, to the total membrane area, A_0, can be expressed by Eq. 8

$$\frac{A_{e,i}}{A_0}=\frac{\left(d_p-d_{k,i}\right)^2}{{d_p}^2} \tag{8}$$

By taking the difference between the pore size and the kinetic diameter of the permeating gas, $d_p-d_{k,i}$, instead of the pore size, d_p, as the effective diffusion length in the GT model for gas permeation in the membrane, a modified GT model is then obtained based on Eq. 2, as shown in Eq. 9

$$P_{m\text{-}GT,i}=\frac{k_{0,i}}{\sqrt{M_i RT}}\exp\left(-\frac{E_{p,i}}{RT}\right) \tag{9}$$

where

$$k_{0,i}=a\left(d_p-d_{k,i}\right)^3 \tag{10}$$

and

$$a=\frac{\sqrt{2\pi}N_p}{6\tau L A_m} \tag{11}$$

Note that when the $d_{k,i}=0$ or together with $E_{p,i}=0$, The modified GT model, Eq. 9, can essentially be converted into

the GT model (Eq. 2) and ideal Knudsen diffusion model (Eq. 1), respectively. For relatively weak-adsorptive gas under the GT region, the apparent activation energy of gas permeation, $E_{p,i}$, in Eq. 9 can be interpreted as the sum of the activation energy of diffusion that is needed to overcome the potential barrier and the adsorption energy under the assumption of the homogeneous potential field inside the pores.[11] $E_{p,i}>0$ and $E_{p,i}<0$ indicates that one diffusion barrier and interaction affinity is more dominative than the other during the permeation process, respectively. When the contribution of the exponential term is negligibly small, Eq. 9 can be rewritten in a simpler form as Eq. 12

$$P_{\text{m-GT},i} \approx \frac{k_{0,i}}{\sqrt{M_i RT}} \tag{12}$$

According to Eq. 9, the pre-exponential factor, $k_{0,i}$, and the activation energy of gas permeation, $E_{p,i}$, can be obtained by fitting the gas permeation data against temperature. a is a structural parameter, which is a constant for a specified membrane regardless of the testing conditions or permeating gases. Therefore, when Eq. 10 is transformed to the following form

$$\sqrt[3]{k_{0,i}} = \sqrt[3]{a} d_p - \sqrt[3]{a} d_{k,i} \tag{13}$$

The parameters between the cubic square root of the pre-exponential factor, $k_{0,i}^{1/3}$, and the kinetic diameter of permeating molecules, $d_{k,i}$, should follow a linear relationship, and the slope and $d_{k,i}$-intercept of this linear function are $-a^{1/3}$and d_p, respectively. Consequently, from the plot of $k_{0,i}^{1/3}$ vs. $d_{k,i}$, both the structural parameter, a, and the pore size of the membrane, d_p, can be effectively quantified.[4]

Based on the modified GT model, a NKP method has been proposed for pore-size evaluation of microporous membranes.[5] NKP is defined by the ratio of an experimental single-gas permeance to a theoretically predicted one that is based on standard gas under a Knudsen diffusion mechanism, as shown in Eq. 14

$$f_{\text{NKP}} = \frac{P_i}{P_s}\sqrt{\frac{M_i}{M_s}} \tag{14}$$

Therefore, when a membrane has a uniform pore size or more generally has a monomodal pore-size distribution, according to Eqs. 9 and 14, the NKP for the i-th component through the membrane can be expressed as follows

$$f_{\text{NKP,mono}} = \left(\frac{d_p - d_{k,i}}{d_p - d_{k,s}}\right)^3 \exp\left(-\frac{E_{p,i} - E_{p,s}}{RT}\right) \tag{15}$$

When the difference in activation energy between the i-th component and the standard gas for gas permeation through the membrane is negligibly small, or when the gas permeation test is performed at a high temperature, then NKP can be further simplified as Eq. 16

$$f_{\text{NKP,mono}} \approx \left(\frac{d_p - d_{k,i}}{d_p - d_{k,s}}\right)^3 \tag{16}$$

In Eq. 16, $d_{k,i}$ and $d_{k,s}$ are known parameters, and the NKP can be easily calculated based on experimentally obtained single-gas permeation data for the membrane. Therefore, in addition to analyzing the plot of $k_{0,i}^{1/3}$ against the $d_{k,i}$ in Eq. 13, the membrane pore size, d_p, can also be readily obtained by fitting the NKP against the kinetic diameter, $d_{k,i}$, in a nonlinear manner for different permeating gases with Eq. 16 for a membrane consisting of a monomodal pore structure.

To clarify the calculation of pore size based on NKP, Eq. 16 is converted into the following form using the cubic root in the equation

$$f_{\text{NKP,mono}}^{1/3} \approx \frac{d_p}{d_p - d_{k,s}} - \frac{d_{k,i}}{d_p - d_{k,s}} \tag{17}$$

Equation 17 shows a linear relationship between the cubic root of NKP and the gas kinetic diameter, $d_{k,i}$. Therefore, the membrane pore size can be obtained from the $d_{k,i}$-intercept by fitting the cubic root of NKP with the gas kinetic diameter in a linear style instead.

In reality, porous membranes with a bimodal pore structure are also very common. For example, defective zeolite membranes consist of two types of pores: intracrystalline and intercrystalline. Therefore, the NKP method used for pore-size calculation should be modified for those membranes with a bimodal pore structure. When a membrane has two types of pores, with sizes $d_{p,1}$ and $d_{p,2}$, and the corresponding number-based pore fractions f_1 and f_2, respectively, the total gas permeance of the i-th component through the membrane, $P_{i,\text{bi}}$, can be expressed as the sum of the values for the gas permeance $P_{i,1}$ and $P_{i,2}$ through the pores $d_{p,1}$ and $d_{p,2}$, respectively, as follows

$$P_{i,\text{bi}} = P_{i,1} + P_{i,2} \tag{18}$$

According to Eq. 9, the values for gas permeance, $P_{i,1}$ and $P_{i,2}$, through the pores with sizes $d_{p,1}$ and $d_{p,2}$, respectively, can be described. Therefore, the total permeance through the entire pores for the i-th component can be further expressed as Eq. 19

$$P_{i,\text{bi}} = \frac{N_p}{6A_m}\sqrt{\frac{2\pi}{M_i RT}}\left(\frac{f_1(d_{p,1} - d_{k,i})^3}{\tau_1 L_1}\exp\left(-\frac{E_{p1,i}}{RT}\right) + \frac{f_2(d_{p,2} - d_{k,i})^3}{\tau_2 L_2}\exp\left(-\frac{E_{p2,i}}{RT}\right)\right) \tag{19}$$

Equation 19 clearly shows how the gas permeation performance of a membrane with a bimodal pore structure is significantly affected by the size and concentration of both types of pores in the membrane, this correlation between the gas permeation properties and pore characteristics would be helpful in understanding how the second type of pore exerts influence on the gas transport behaviors of membranes.

When either the absolute values of the activation energies for gas permeation through both types of pores are very small or the gas permeation is carried out at a high temperature, the exponential terms in Eq. 19 would be negligible. When the same membrane thickness and tortuosity is assumed for two types of pores, Eq. 19 can be simplified as Eq. 20

$$P_{i,\text{bi}} \approx \frac{N_p}{6\tau A_m L}\sqrt{\frac{2\pi}{M_i RT}}\left(f_1(d_{p,1} - d_{k,i})^3 + f_2(d_{p,2} - d_{k,i})^3\right) \tag{20}$$

Based on Eq. 14, the NKP of the i-th component for a membrane with a bimodal pore structure can be expressed as follows

$$f_{\text{NKP,bi}} \approx \frac{f_1(d_{p,1} - d_{k,i})^3 + f_2(d_{p,2} - d_{k,i})^3}{f_1(d_{p,1} - d_{k,s})^3 + f_2(d_{p,2} - d_{k,s})^3} \tag{21}$$

Moreover, for a bimodal pore structure

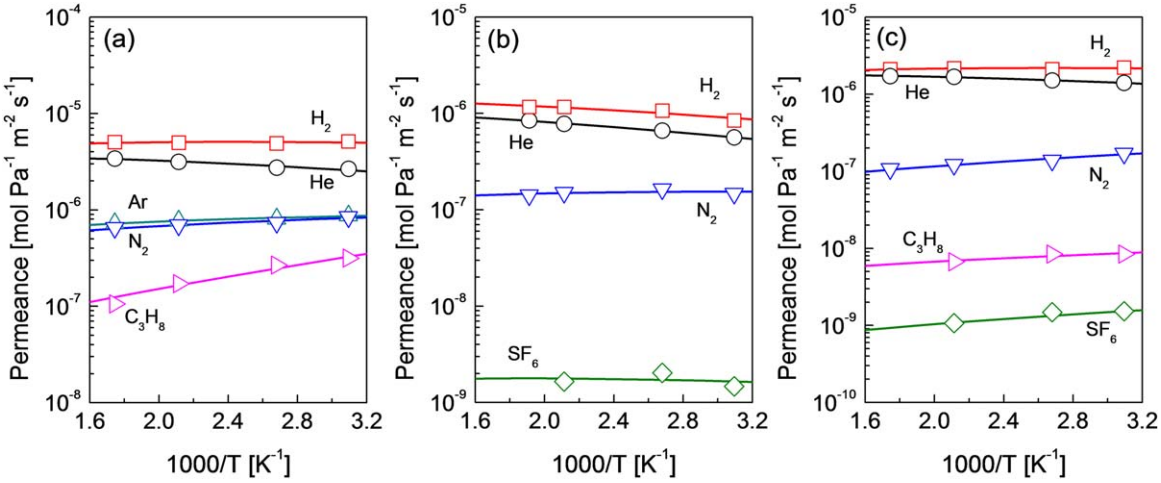

Figure 1. Temperature dependence of gas permeance for (a) BTESE-, (b) TEDMDS-, and (c) HEDS-derived silica membranes.

Symbols are experimental; curves are calculated using Eq. 9. [Color figure can be viewed in the online issue, which is available at wileyonlinelibrary.com.]

$$f_2 = 1 - f_1 \tag{22}$$

Therefore, the expression of NKP in Eq. 21 can be transformed to the following form

$$f_{\mathrm{NKP,bi}} \approx \frac{(1-f_2)\left(d_{\mathrm{p},1}-d_{\mathrm{k},i}\right)^3 + f_2\left(d_{\mathrm{p},2}-d_{\mathrm{k},i}\right)^3}{(1-f_2)\left(d_{\mathrm{p},1}-d_{\mathrm{k,s}}\right)^3 + f_2\left(d_{\mathrm{p},2}-d_{\mathrm{k},s}\right)^3} \tag{23}$$

As with the aforementioned discussion, when a membrane consists of a multimodal pore structure, the gas permeance and NKP can be expressed as follows

$$P_{i,\mathrm{mutil}} = \frac{N_{\mathrm{p}}}{6\tau A_{\mathrm{m}} L}\sqrt{\frac{2\pi}{M_i RT}}\left(\sum_m f_m\left(d_{\mathrm{p},m}-d_{\mathrm{k},i}\right)^3 \exp\left(-\frac{E_{\mathrm{p}m,i}}{RT}\right)\right) \tag{24}$$

When either the activation energies are negligible or the gas permeation is performed under a high temperature, the gas permeance and NKP can be expressed as Eqs. 25 and 26, respectively

$$P_{i,\mathrm{mutil}} \approx \frac{N_{\mathrm{p}}}{6\tau A_{\mathrm{m}} L}\sqrt{\frac{2\pi}{M_i RT}}\left(\sum_m f_m\left(d_{\mathrm{p},m}-d_{\mathrm{k},i}\right)^3\right) \tag{25}$$

$$f_{\mathrm{NKP,multi}} \approx \frac{\sum_m f_m\left(d_{\mathrm{p},m}-d_{\mathrm{k},i}\right)^3}{\sum_m f_m\left(d_{\mathrm{p},m}-d_{\mathrm{k,s}}\right)^3} \tag{26}$$

Experimental

Materials

Bis(triethoxysilyl)ethane (BTESE) and 1,1,3,3-tetraethoxy-1,3-dimethyldisiloxane (TEDMDS) were purchased from Gelest. Ethanol, tetraethoxysilane, hydrochloric acid, and acetic acid were supplied by Sigma-Aldrich. Hexaethoxydisiloxane (HEDS) was synthesized according to a previously reported procedure.[12]

Membrane preparation

Various silica sols were prepared by acid-catalyzed hydrolysis and polymerization of BTESE, TEDMDS, and HEDS in a water and ethanol mixture via sol-gel processing, as reported previously.[5,12,13] A porous α-alumina tube (NOK, Japan) (outer diameter: 3.0 mm; pore size: 100 nm) was used as a support for membrane preparation. First, a SiO_2–ZrO_2 intermediate layer was deposited onto the support, resulting in a smooth surface and a pore size reduced to several nanometers. The separation layer was fabricated by coating the silica sols onto the intermediate layer, with subsequent calcination at 350–550°C under either a N_2 or an air atmosphere. The above procedure for the deposition of a silica layer was repeated twice to form a continuous separation layer.

Single-gas permeation measurements

Gas permeation through the membranes was performed at 50–300°C using single components of He, H_2, Ar, CH_4, C_3H_8, and SF_6 with pressures on the feed and permeant sides fixed at 200 and 100 kPa. Prior to the measurements, all membranes were treated in a He flow overnight at 200°C to remove the adsorbed water in the membrane pores. The gas flows that permeated the membranes were measured using a bubble flow meter (Horiba, Japan). A schematic representation of the experimental setup for gas permeation was shown in a previous study.[5]

Results and Discussion

Pore-size evaluation of microporous membranes

Figure 1 shows the temperature dependence of gas permeance for BTESE-, TEDMDS-, and HEDS-derived silica membranes. Almost all the values for gas permeance through the membranes were only slightly temperature-dependent. This shows that the interaction between the gas molecules and the pore walls of membranes was not very strong, thus, the absolute values of the activation energies for gas permeation in these membranes should be small. For clarity, the activation energies and pre-exponential factors for gas permeation through the membranes were calculated by regressing the temperature dependence of gas permeance with Eq. 9, and the obtained results are listed in Table 1. The activation energies for gas permeation in BTESE- and HEDS-derived silica membranes ranged from −2 to 3 kJ mol^{-1}, and

Table 1. Pre-Exponential Factors ($k_{0,i}$) and Activation Energies ($E_{p,i}$) for Gas Permeation Through BTESE-, TEDMDS-, and HEDS-Derived Silica Membranes

Gas	Kinetic Diameter $d_{k,i}$ (nm)	BTESE		TEDMDS		HEDS	
		$k_{0,i} \times 10^4$ (−)	$E_{p,i}$ (kJ mol^{-1})	$k_{0,i} \times 10^4$ (−)	$E_{p,i}$ (kJ mol^{-1})	$k_{0,i} \times 10^4$ (−)	$E_{p,i}$ (kJ mol^{-1})
He	0.26	9.46	3.39	3.08	4.46	4.55	3.07
H_2	0.289	6.91	1.70	2.65	3.75	2.83	1.55
Ar	0.346	3.64	0.69	–	–	–	–
N_2	0.364	2.44	0.21	0.70	1.33	0.31	−1.05
C_3H_8	0.43	0.24	−4.18	–	–	0.03	−0.30
SF_6	0.55	–	–	0.02	2.21	0.006	−1.29

gas permeation in TEDMDS-derived silica membrane also showed relatively low values that ranged from 1 to 5 kJ mol^{-1}. Prior to the analysis of membrane pore size using the NKP method, it is important to estimate the activation energies for gas permeation, because a relatively small difference in the activation energies among the permeating gases enables the simple evaluation of membrane pore size using the NKP method, according to Eq. 15. Moreover, the values of the pre-exponential factors obtained in the fitting also are crucial, because these are the key parameters required for the evaluation of the membrane pore size in the plot of $k_{0,i}^{1/3}$ against the kinetic diameter.

As derived from the modified GT model, both the plots of $k_{0,i}^{1/3}$ and $f_{NKP}^{1/3}$ against the kinetic diameter of a permeating gas could be used to analyze the pore sizes of microporous membranes. By comparing the basic Eqs. 13 and 17, pore size could be more precisely estimated using the $k_{0,i}^{1/3}$ plot rather than the $f_{NKP}^{1/3}$ plot, as the $f_{NKP}^{1/3}$ plot did not take into consideration the effect of activation energy on NKP. However, the NKP method required much less experimental data to estimate membrane pore size, which made its application much simpler and more convenient than that of the $k_{0,i}^{1/3}$ plot. When using the NKP method, to increase the accuracy of the pore-size calculation, the fitting of the experimentally obtained data with the gas kinetic diameter is usually performed across a wide range under a limiting condition of $d_{k,s} < d_{k,i} < d_p$. Therefore, He, which has the smallest molecular size, was generally used as the standard gas in previous studies.[4,5,8–10] Considering the small molecular size, H_2 would be another good candidate for the standard gas in the NKP method. Therefore, to gain insight into the effects of the activation energy and the standard gas on pore-size evaluation, three membranes were analyzed using He- and H_2-standard-gas-based $f_{NKP}^{1/3}$ plots together with $k_{0,i}^{1/3}$ plots for a comparative study.

Figures 2 and 3 show the plots of $f_{NKP}^{1/3}$ and $k_{0,i}^{1/3}$, respectively, against the kinetic diameter for an evaluation of the pore sizes of three silica membranes, and the results are summarized in Table 2. Pore sizes obtained by fitting the experimental data with Eq. 17 for all permeating gases were 0.650, 0.655, and 0.557 nm for BTESE-, TEDMDS-, and HEDS-derived silica membranes, respectively, in the He-standard-gas-based $f_{NKP}^{1/3}$ plot (Solid lines in Figure 2a), while the H_2-standard-gas-based $f_{NKP}^{1/3}$ plot indicated that the corresponding membranes had slightly smaller pore sizes of 0.611, 0.633, and 0.554 nm (Solid lines in Figure 2b), respectively. These small differences in the pore-size estimation could be ascribed to the activation energy of H_2 being smaller than that of He in these membranes, which, according to Eq. 15, reduced the effect of activation energy on the NKP. These similar pore sizes suggest that H_2 could be used as an alternative standard gas when plotting the $f_{NKP}^{1/3}$ against kinetic diameter for pore-size evaluation. Furthermore, the calculated pore sizes approximate those obtained from the

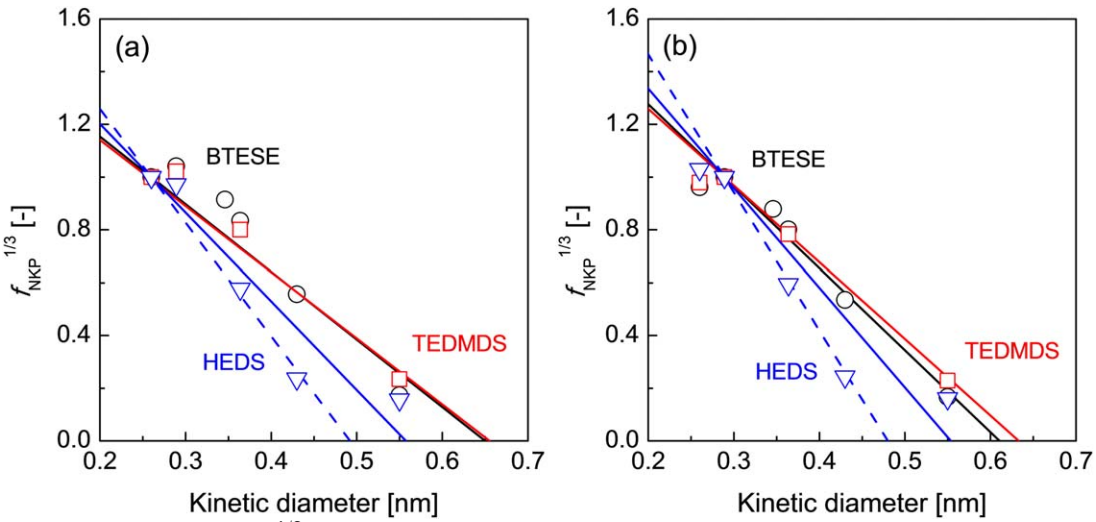

Figure 2. Relationships between $f_{NKP}^{1/3}$ and the gas kinetic diameter for BTESE-, TEDMDS-, and HEDS-derived silica membranes using (a) He and (b) H_2 as the standard gas.

Symbols are experimental; curves were calculated using Eq. 17. [Color figure can be viewed in the online issue, which is available at wileyonlinelibrary.com.]

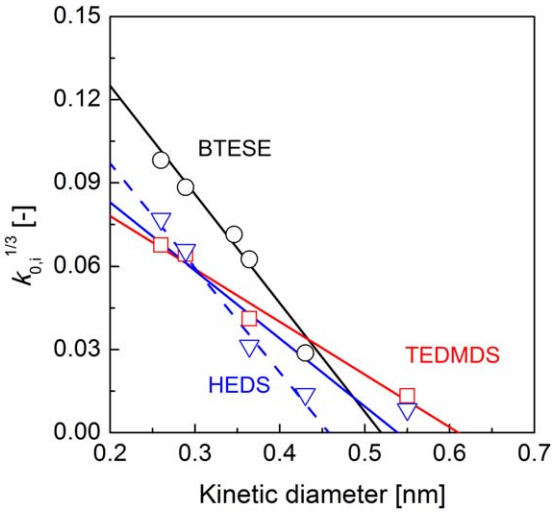

Figure 3. Relationships between $k_{0,i}^{1/3}$ and the gas kinetic diameter for BTESE-, TEDMDS-, and HEDS-derived silica membranes.

Symbols are experimental; curves were calculated using Eq. 13. [Color figure can be viewed in the online issue, which is available at wileyonlinelibrary.com.]

plot of $k_{0,i}^{1/3}$ (Solid lines in Figure 3) (0.512, 0.611, and 0.539 nm for BTESE-, TEDMDS-, and HEDS-derived silica membranes, respectively), which are thought to be theoretically accurate as the activation energy has no adverse effects on the pore-size calculation, indicating that the simple evaluation of membrane pore sizes based on the plot of $f_{\mathrm{NKP}}^{1/3}$ against the gas kinetic diameter is applicable when the small activation energies for gas permeation are ignored.

It should be noted that, compared with the BTESE- and TEDMDS-derived silica membranes, relatively large deviations were observed between the experimentally obtained data and the theoretical lines in the plots for both $f_{\mathrm{NKP}}^{1/3}$ (Figure 2) and $k_{0,i}^{1/3}$ (Figure 3) for the HEDS-derived silica membrane. When the permeation data of SF_6 was not considered in the fitting, an obviously different theoretical line (dotted lines in Figures 2 and 3) was obtained for the HEDS-derived silica membrane in the plots of $f_{\mathrm{NKP}}^{1/3}$ and $k_{0,i}^{1/3}$ that showed a very good correlation with the experimental data except for SF_6. Theoretically, if a membrane has a uniform pore size, a linear relationship between the $f_{\mathrm{NKP}}^{1/3}$ and the kinetic diameter should follow for all permeating gases, as observed for BTESE- and TEDMDS-derived silica membranes. The deviation of SF_6 indicated the presence of a rather broad pore-size distribution in the HEDS-derived silica membrane. For the HEDS-derived silica membrane, the experimentally obtained values of $f_{\mathrm{NKP}}^{1/3}$ and $k_{0,i}^{1/3}$ for SF_6 were much higher than the theoretically predicted ones (dotted lines in Figures 2 and 3), indicating additional permeation through the membrane. This could be ascribed to the presence of a few pinholes in the HEDS-derived silica membrane. From the $d_{\mathrm{k},i}$-intercept in the $f_{\mathrm{NKP}}^{1/3}$ or $k_{0,i}^{1/3}$ plots, it can be concluded that the HEDS-derived silica membrane was composed of a massive number of pores around 0.459 nm and a few pinholes that were larger than SF_6 (0.55 nm). Obviously, SF_6 permeation through the membrane mainly occurred in the pinholes, because the molecular size of SF_6 was too large to permeate the 0.459 nm pores in the membrane. Conversely, the smaller gases, such as He, H_2, N_2, and C_3H_8, were supposed to mainly permeate the pores that were approximately 0.459 nm, and the effect of the pinholes on their permeation was thought to be negligible, because of a very limited number of pinholes, as confirmed by a very good linear correlation between the experimentally obtained data and the theoretical lines for the gases that were smaller than SF_6. Previously, similar multiple theoretical lines were also reported for a DDR zeolite membrane when fitting different groups of permeating gases by Yoshioka et al.,[4] and the cause of the multiple theoretical lines was ascribed to the presence of intercrystalline pores in the DDR-type zeolite membrane. Obviously, the study on the $f_{\mathrm{NKP}}^{1/3}$ and $k_{0,i}^{1/3}$ plots provides a novel and effective route to gain new insights into the microstructures and gas permeation characteristics of microporous membranes. It should be noted that, in this work, the use of the $f_{\mathrm{NKP}}^{1/3}$ plot instead of the previously reported[4,5,8–10] f_{NKP} plot against the gas kinetic diameter allowed us to obtain both the pore size and details about the pore structures and gas permeation of the membranes.

Table 2. Calculated Pore Sizes for BTESE-, TEDMDS-, and HEDS-Derived Silica Membranes

	Calculated Pore Size, d_p (nm)		
Membrane	$f_{\mathrm{NKP}}^{1/3}$ plot (He)	$f_{\mathrm{NKP}}^{1/3}$ plot (H_2)	$k_{0,i}^{1/3}$ plot
BTESE	0.650	0.611	0.512
TEDMDS	0.655	0.633	0.611
HEDS	0.557	0.554	0.539
	0.492[a]	0.480[a]	0.459[a]

[a]Pore sizes calculated without consideration of SF_6 permeation for the HEDS-derived silica membrane.

Gas transport behaviors of microporous membranes with a uniform pore size

Considerable effort has been devoted to the application of microporous membranes for gas separation, particularly for some important processes such as CO_2/CH_4 and O_2/N_2 separations. However, the effective separation of these gas pairs by porous membranes is challenging, because the difference in their molecular sizes is small (CO_2: 0.33 nm, CH_4: 0.38 nm, O_2: 0.34 nm, N_2: 0.364), and the membrane pore size is difficult to control in such a narrow range. Theoretically, when a membrane has a uniform pore size that is between the molecular sizes of the gas pairs of CO_2/CH_4 or O_2/N_2, it means no CH_4 and N_2 permeation through the membrane for CO_2/CH_4 and O_2/N_2 separations, respectively, and infinite selectivity can be obtained under this circumstance. However, when the membrane pore size is larger than the molecular sizes of both permeating gases, the gas pairs can simultaneously permeate through the membrane. Obviously, to effectively separate the gas mixtures, the pore size of the membrane must be controlled to within a reasonable range. However, the quantitative effect of membrane pore size on gas-separation performance has not yet been clarified. For a membrane with a uniform pore size, according to Eq. 9, the ideal selectivity of the i-th to the j-th component, $\alpha_{i/j}$, can be expressed as the single permeance ratio, as follows[14]

$$\alpha_{i/j,\mathrm{mono}}=\sqrt{\frac{\overline{M}_j}{M_i}}\frac{\left(d_{\mathrm{p}}-d_{\mathrm{k},i}\right)^3}{\left(d_{\mathrm{p}}-d_{\mathrm{k},j}\right)^3}\exp\left(-\frac{E_{\mathrm{p},i}-E_{\mathrm{p},j}}{RT}\right) \quad (27)$$

For a specified separation system operated at a constant temperature, Eq. 27 clearly shows that the ideal selectivity

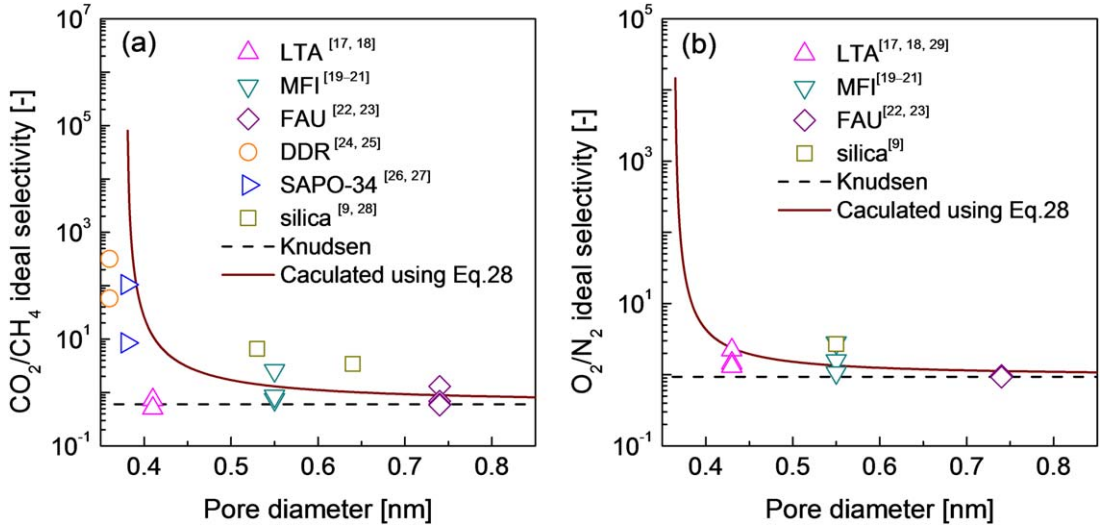

Figure 4. Experimental and calculated (a) CO_2/CH_4 and (b) O_2/N_2 ideal selectivities for microporous membranes with different pore sizes.

[Color figure can be viewed in the online issue, which is available at wileyonlinelibrary.com.]

for a membrane is affected by both the pore size of the membrane and the differences in the activation energies for gas permeation. This result indicates that, in the GT region, in addition to pore-size control, increasing the affinity of membrane matrix to CO_2 is another feasible route toward improving membrane selectivity, particularly under a relatively low operating temperature. Much effort has been made to develop new membrane materials with a high affinity to CO_2 for enhanced CO_2 separation.[15,16]

When either the difference in the activation energies for gas permeation is small or membrane separation is operated at a high temperature, the effect of the exponential term in Eq. 27 on the membrane selectivity becomes insignificant, and, thus, the ideal selectivity of the membrane can be approximately expressed using Eq. 28

$$\alpha_{i/j,\text{mono}} \approx \sqrt{\frac{M_j}{M_i}} \frac{\left(d_p - d_{k,i}\right)^3}{\left(d_p - d_{k,j}\right)^3} \tag{28}$$

Equation 28 shows that the ideal selectivity is dependent only on the pore size of the membrane for a given separation system under high temperatures, and it decreases with increases in the pore size when the kinetic diameter of the i-th component is smaller in the separation system. This indicates that the preparation of membranes with a controllable size is much more important for gas separation at high temperatures. Furthermore, according to Eq. 28, the ideal selectivity of a membrane can be predicted for a binary separation system when the pore size of a membrane is already known. Figure 4 shows the predicted and experimental ideal selectivities of CO_2/CH_4 and O_2/CH_4 as a function of membrane pore size. The predicted curves show that the selectivities of CO_2/CH_4 and O_2/N_2 decreased rapidly with increases in membrane pore size and finally approximated Knudsen selectivity, which suggests that the membrane selectivity was very sensitive to pore size. The reported[9,17–29] experimental selectivities of various microporous membranes that were obtained at temperatures above 100°C (~30°C for FAU-type zeolite membranes) against their pore sizes are also plotted in Figure 4. Both the experimental results and the theoretical curves showed an acceptable degree of CO_2/CH_4 and O_2/N_2 separation, although the effect of activation energy for gas permeation and the presence of defects in the membrane could lead to some deviations. This confirms that Eq. 28 is effective when calculating the optimal membrane pore size for target selectivity. For example, to obtain CO_2/CH_4 and O_2/N_2 selectivities of more than 100 and 30, respectively, at a high temperature, membrane pore sizes smaller than 0.391 and 0.375 nm, respectively, are preferable. The application of Eq. 28 can also be extended to other separation systems, either for the selection of a membrane with an appropriate pore size to fulfill a specified separation task or to predict separation performance for a membrane with a given pore size.

Gas transport behaviors of defective microporous membranes

It is well known that the existence of defects in membranes may significantly affect the membrane performance, even though the concentration may be small and the size may be in the nanometer range. To gain insight into the effect of nano-sized defects on a membrane performance, two theoretical membranes, M-1 and M-2, were selected for a comparative study. Note that, M-1 and M-2 represent typical silica and MFI zeolite membranes, which have intrinsic pore sizes of 0.34 and 0.55 nm, respectively. The defect concentration in the membranes was defined by the ratio of the numbers of defective pores to total pores for gas permeation. For simplification, the defects in both membranes were assumed to be 1 nm uniform pores. Therefore, the defective membranes could be thought of as ideal bimodal pore structures. Figure 5 shows the effect of defect concentration on the gas permeance through membranes M-1 and M-2 as a function of the kinetic diameter of the permeating gas. All values for gas permeance in Figure 5 were theoretically calculated at a high temperature using Eq. 20, and then were further normalized by the He permeance through the corresponding membrane without defects ($f_2 = 0$). As the defect concentration increased in the membranes, gas permeance

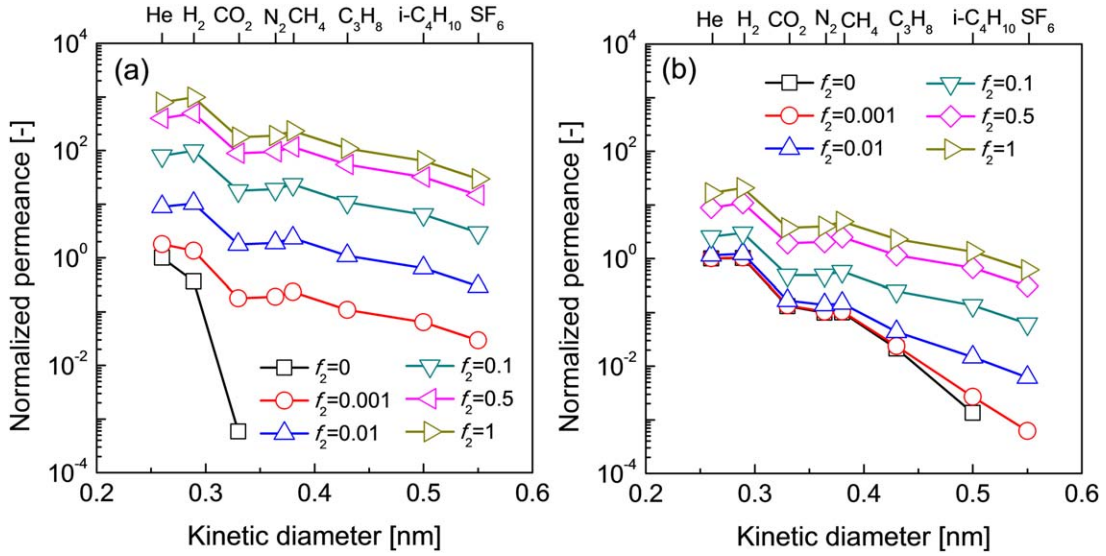

Figure 5. Kinetic diameter dependence of gas permeance for microporous membranes (a) M-1 ($d_{p,1} = 0.34$ nm) and (b) M-2 ($d_{p,1} = 0.55$ nm) with different defect concentrations ($d_{p,2} = 1$ nm).

Curves were calculated using Eq. 20. [Color figure can be viewed in the online issue, which is available at wileyonlinelibrary.com.]

through both membranes gradually increased while membrane selectivity decreased. This phenomenon was much more remarkable for M-1, which had a smaller original pore size of 0.34 nm. For example, when both membranes had defective pores of 1 nm with a concentration of 10^{-3}, the gas permeance, particularly for gas molecules larger than CO_2, were obviously increased for M-1, and this led to a drastic decrease in the membrane selectivity for M-1. However, M-2 had a medium pore size of 0.55 nm, and all permeance values were approximately unchanged, resulting in a selectivity that was comparable to a membrane with no defects. These results show that the presence of nano-sized defects can more easily deteriorate the gas-separation performance for a membrane with a smaller pore size. As the original membrane pore size was decreased, the percentage of gas that would permeate the original pores was less, while the percentage of gas permeation occurred in the defects became more, resulting in a loss in membrane selectivity.

Figure 6 shows the effect of defect concentration on He-standard-gas-based f_{NKP} as a function of kinetic diameter for membranes M-1 and M-2. Compared with the f_{NKP} plot for M-1 and M-2 with $f = 0$, when both membranes had a low defect concentration, such as $f = 0.001$ or 0.01, the theoretical curves changed significantly for M-1, while there was only a slight change for M-2. This result again confirms that the presence of defects exerts a very important influence on the gas permeation properties of a membrane with a small pore size, although the concentration is small. With a further increase in the defect concentration in both membranes, the change in theoretical curves was no longer obvious for M-1, indicating that defective pores dominated the membrane performance. Conversely, the theoretical curves still showed

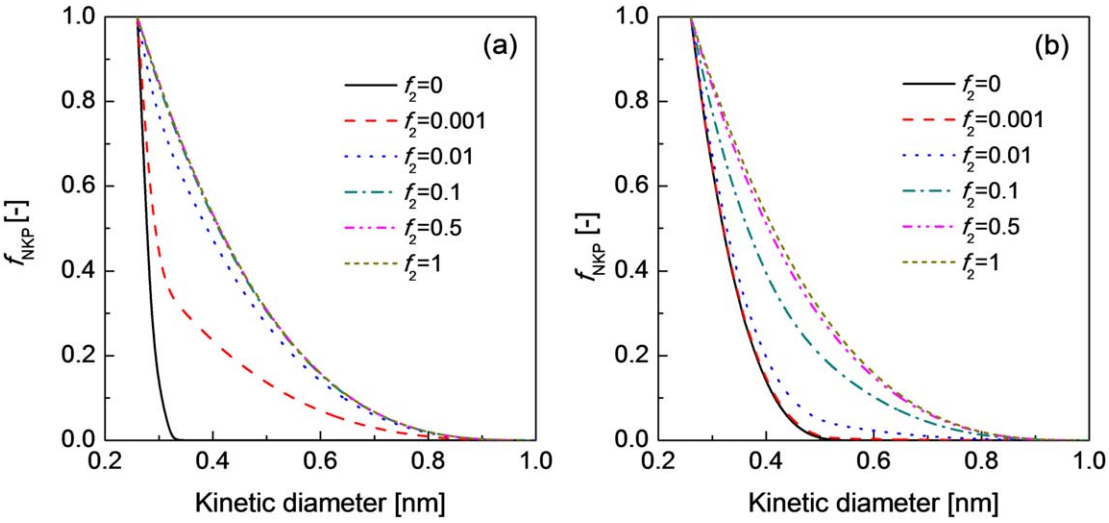

Figure 6. Effect of defect concentration ($d_{p,2} = 1$ nm) on He-standard-gas-based f_{NKP} as a function of kinetic diameter for membranes (a) M-1 ($d_{p,1} = 0.34$ nm) and (b) M-2 ($d_{p,1} = 0.55$ nm).

Curves were calculated using Eq. 21. [Color figure can be viewed in the online issue, which is available at wileyonlinelibrary.com.]

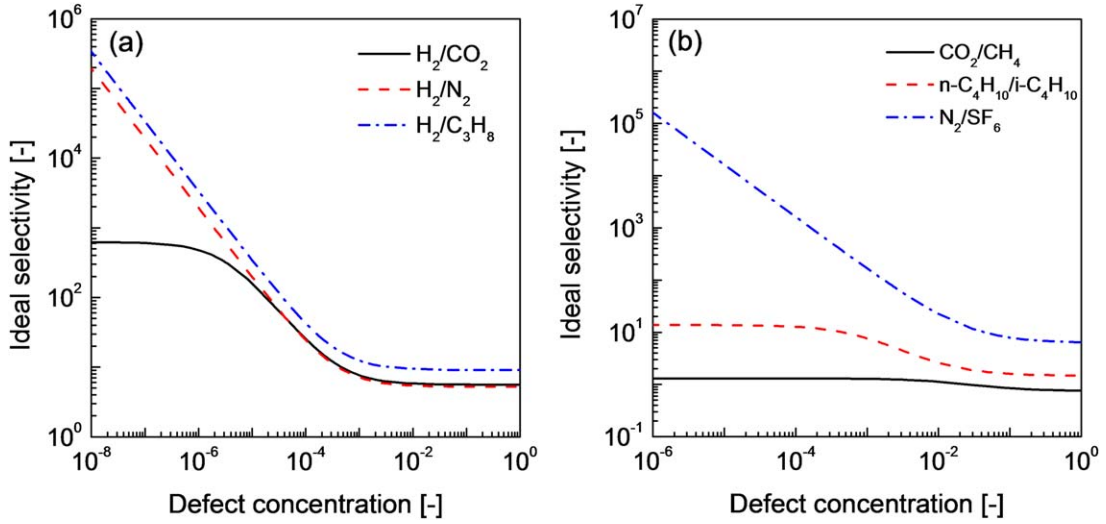

Figure 7. Effect of defect concentration ($d_{p,2} = 1$ nm) on gas-separation performance for membranes (a) M-1 ($d_{p,1} = 0.34$ nm) and (b) M-2 ($d_{p,1} = 0.55$ nm).

Curves were calculated using Eq. 29. [Color figure can be viewed in the online issue, which is available at wileyonlinelibrary.com.]

some obvious changes for M-2, suggesting that both the original and the defective pores in M-2 had an important effect on the gas permeation properties. The evolution of the f_{NKP} plots for M-1 and M-2 with different defect concentrations further shows that the effect of the defects on gas permeation properties largely depended on the original pore sizes of the membranes.

According to Eq. 20, the ideal selectivity of i-th to j-th components through a membrane with a bimodal pore structure can be denoted as follows

$$\alpha_{i/j,\mathrm{bi}} \approx \sqrt{\frac{M_j}{M_i}} \frac{(1-f_2)\left(d_{\mathrm{p},1}-d_{\mathrm{k},i}\right)^3+f_2\left(d_{\mathrm{p},2}-d_{\mathrm{k},i}\right)^3}{(1-f_2)\left(d_{\mathrm{p},1}-d_{\mathrm{k},j}\right)^3+f_2\left(d_{\mathrm{p},2}-d_{\mathrm{k},j}\right)^3} \tag{29}$$

Note that, when the $f_2 = 0$ or 1, which corresponds to a membrane with a monomodal pore structure, Eq. 29 can be finally converted to Eq. 28, which is used to describe the ideal selectivity for a membrane with a monomodal pore structure. Figures 7a, b show the effect of the presence of 1 nm defective pores in membranes M-1 and M-2 on their gas-separation performance. As membranes M-1 and M-2 have a small pore size of 0.34 nm and a medium pore size of 0.55 nm, respectively, M-1 was studied for H_2 separation, while M-2 was used for the separation of relatively larger gas molecules, such as CO_2, N_2, and n-C_4H_{10} (0.43 nm) separation from CH_4, SF_6, and i-C_4H_{10} (0.5 nm), respectively. Among the separation systems studied, H_2/N_2, H_2/C_3H_8, and N_2/SF_6 separation through the corresponding membrane without the presence of defective pores should theoretically have an infinite degree of selectivity, because N_2, C_3H_8, and SF_6 are impermeable. With increases in the defect concentration of a membrane, the ideal selectivities of H_2/N_2 and H_2/C_3H_8 for M-1 initially decreased rapidly due to the enhanced permeation of N_2 and C_3H_8, and then the ideal selectivities remained approximately at the Knudsen values when the defects concentration was larger than 10^{-3}, because the gas permeation was then dominated by the 1 nm defective pores. Conversely, a small defect concentration would have almost no effect on the H_2/CO_2 selectivity, as the permeation of CO_2 still mainly occurs in the 0.34 nm pores in M-1 due to a significantly large number of pores that are larger than the size of CO_2. When the defect concentration was increased from $\sim 10^{-6}$ to 10^{-3}, defective pores in M-1 had an obvious impact on the CO_2 permeation in M-1, resulting in a decrease in H_2/CO_2 selectivity. With further increases in the defect concentration, there were almost no changes in the H_2/CO_2 selectivities, which remained at approximately the Knudsen value, because most of the H_2 and CO_2 permeated through the defects rather than through the original pores under a high defect concentration. For CO_2/CH_4 and n-C_4H_{10}/i-C_4H_{10} separation by membrane M-2 with an original pore size of 0.55 nm, the selectivities were quite low even at an extremely small defect concentration, because all gases easily permeated the membrane owing to the relatively large membrane pore size. The separation of a N_2/SF_6 mixture by membrane M-2 was much more efficient, and the N_2/SF_6 selectivities decreased remarkably as the concentration of defective pores increased, for reasons similar to those described for the H_2/N_2 and H_2/C_3H_8 separations by membrane M-1. Eliminating the defective pores is a well-known key to obtaining an excellent molecular sieving effect for microporous membranes, and the above discussion clearly demonstrates this challenge in the preparation of high-performance gas-separation membranes for use at high temperatures.

Figure 8 shows the effect of membrane defects on H_2/SF_6 separation for membranes M-1 and M-2. The H_2/SF_6 selectivities of both membranes decreased rapidly with increases in the defects concentration, and then gradually approached Knudsen selectivity. However, with a defect concentration lower than 10^{-3}, membrane M-2 showed a H_2/SF_6 selectivity that was approximately two orders of magnitude higher than that of membrane M-1. This is because membrane M-2 had a larger pore size of 0.55 nm that allowed a much higher degree of H_2 permeation flux, while the permeation of SF_6 only occurred in the membrane defects. This result illustrates how a larger membrane pore size helps to increase the membrane selectivity for binary gas separation, when the larger gas component permeates only through the membrane defects.

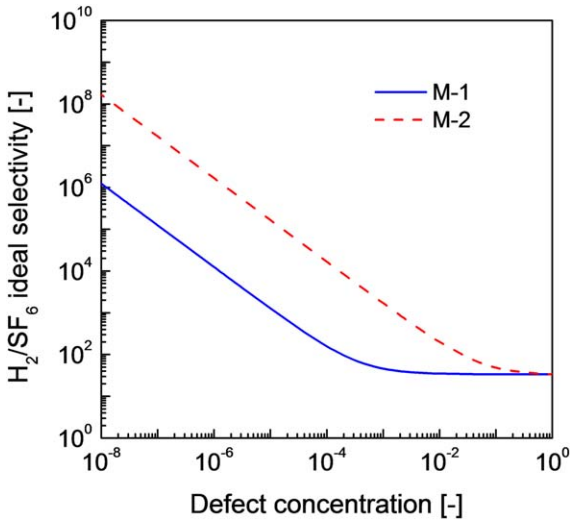

Figure 8. Effect of defect concentration ($d_{p,2} = 1$ nm) on the H_2/SF_6 separation for membranes M-1 ($d_{p,1} = 0.34$ nm) and M-2 ($d_{p,1} = 0.55$ nm).

Curves were calculated using Eq. 29. [Color figure can be viewed in the online issue, which is available at wileyonlinelibrary.com.]

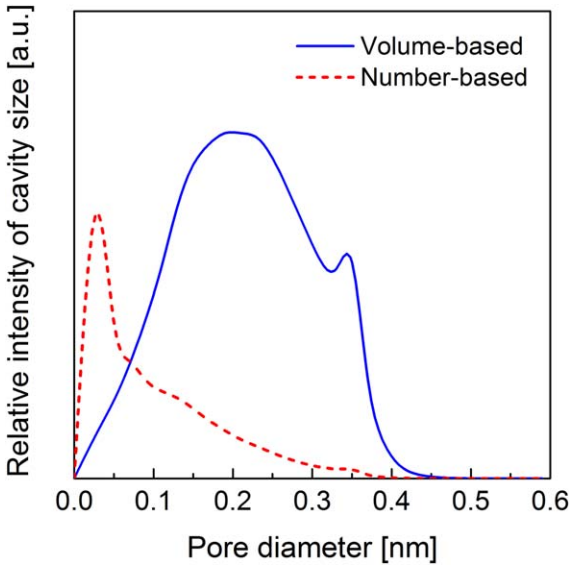

Figure 9. Pore-size distribution of a microporous silica membrane.

[Color figure can be viewed in the online issue, which is available at wileyonlinelibrary.com.]

Gas transport behaviors of microporous membranes with a pore-size distribution

Unlike high-quality zeolite membranes with an extremely uniform pore size, amorphous silica membranes have a relatively broad pore-size distribution. A previous simulation study[30] had demonstrated that the pore size of a silica membrane could range from 0 to several angstroms, as shown in Figure 9. Because considerable pores in the silica network were too small to allow gas permeation, pore sizes smaller than the kinetic diameter of He (0.26 nm) were thus not considered in the following calculation. To study the pore-size distribution on the f_{NKP} plot and gas permeation properties, the mean pore size of a silica membrane was defined in Eq. 30 based on equal pore area and pore numbers

$$d_{p,mean} = \sqrt{\frac{\sum_m N_{p,m} d_{p,m}^2}{\sum_m N_{p,m}}} \tag{30}$$

According to Eq. 30, an ideal silica membrane (denoted as M-3) was assumed to have an entirely uniform pore size that is identical to the mean pore size of a theoretical silica membrane (denoted as M-4) with a pore-size distribution shown in Figure 9 for the following study.

Figure 10 shows the relationships between He-standard-gas-based f_{NKP} and the gas kinetic diameter for membranes M-3 and M-4, based on Eqs. 16 and 26, respectively. The theoretical curves for membranes M-3 and M-4 were similar, indicating the mean pore size of M-4 was very close to that of M-3. When the kinetic diameter of the permeating gas was smaller than 0.32 nm, the values of f_{NKP} for M-3 were only slightly higher than those for M-4, showing that the pore-size distribution in the membrane had only a slight affect on the gas permeation properties for small gas molecules. However, when the kinetic diameter of the permeating gas was larger than 0.32 nm, the values of f_{NKP} for M-4 with a pore-size distribution became slightly larger than those for M-3 with uniform pores, and the differences in the values of f_{NKP} seemed more obvious as the kinetic diameter of the permeating gases was increased. This demonstrates that the pore-size distribution in a silica membrane has a more significant affect on the gas permeation performance of larger gas molecules.

Figure 11 shows the kinetic diameter dependence of gas permeance for the membranes M-3 and M-4. The values for gas permeance were obtained using Eqs. 12 and 25 and were then normalized by the He permeance through the corresponding membrane. The small permeating gases, such as He, H_2, and Ar, showed almost the same dimensionless permeance for both M-3 and M-4 regardless of the pore-size distribution in the membranes. Therefore, both membranes showed almost the same selectivities for the separation of

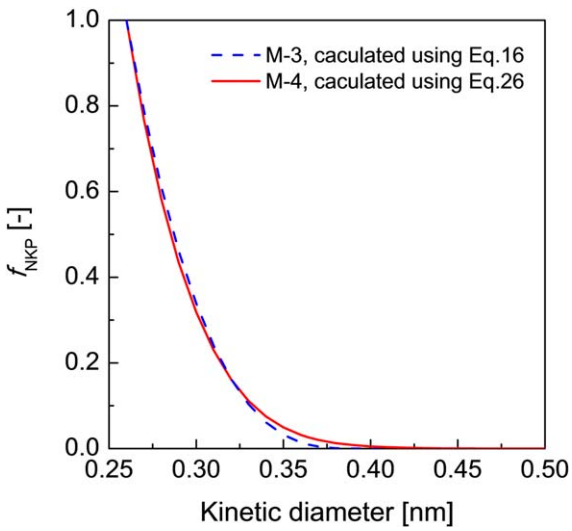

Figure 10. Relationships between He-standard-gas-based f_{NKP} and the gas kinetic diameter for membranes M-3 and M-4.

[Color figure can be viewed in the online issue, which is available at wileyonlinelibrary.com.]

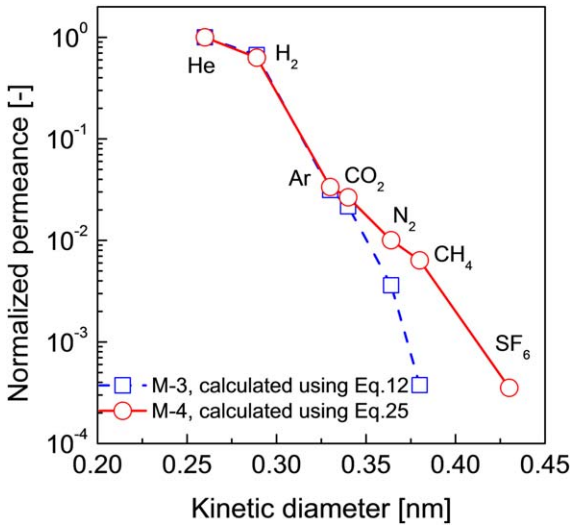

Figure 11. Kinetic diameter dependence of gas permeance for membranes M-3 and M-4.

[Color figure can be viewed in the online issue, which is available at wileyonlinelibrary.com.]

small gas pairs. However, the values for gas permeance of relatively larger gas molecules, such as CO_2, N_2, CH_4, and C_3H_8, were obviously higher for M-4, and this trend was much more remarkable as the kinetic diameter of the permeating gas increased, resulting in decreased membrane selectivity for large gas molecules. This gas permeation result is consistent with that reflected by the f_{NKP} plot in Figure 10. Because the large gas molecules mainly permeated the large pores in a membrane, the difference in the gas permeation properties between M-3 and M-4 could be ascribed mainly to the relatively large pores in the pore-size distribution, although the number of the large pores was small. Obviously, when membrane selectivity is taken into consideration, a silica membrane with a relatively uniform pore size is preferable for gas separations, particularly for the separation from the relatively large gas molecules.

Conclusions

A modified GT model was applied to pore-size evaluation and to the study of the gas transport behaviors of microporous membranes. The plots for $f_{NKP}^{1/3}$ and $k_{0,i}^{1/3}$, as a function of the kinetic diameter of permeating gas, were used to analyze the pore sizes of microporous membranes and were compared based on the gas permeation data of three silica membranes that were derived from different alkoxides. In addition, gas transport through membranes with a uniform pore size, the presence of defective pores, and pore-size distributions were theoretically investigated.

1. Three silica membranes derived from BTESE, TEDMDS, and HEDS were prepared via a sol-gel processing. Values for the temperature dependence of gas permeance for the three silica membranes showed relatively small activation energies that ranged from -4 to 5 kJ mol^{-1}, and more typically in the range of -1–3 kJ mol^{-1}.

2. The pore sizes obtained for the three silica membranes were studied by plotting $f_{NKP}^{1/3}$ and $k_{0,i}^{1/3}$ against the gas kinetic diameter. In the $f_{NKP}^{1/3}$ plot, the pore sizes for BTESE-, TEDMDS-, and HEDS-derived silica membranes were 0.650, 0.655, and 0.557 nm, respectively, using He as the standard gas; Using H_2 as the standard gas gave the corresponding membranes similar pore sizes of 0.611, 0.633, and 0.554 nm, respectively, and those values were also very close to the conclusions obtained from the $k_{0,i}^{1/3}$ plot (0.512, 0.611, and 0.539 nm). These results indicate that H_2 can be used as an alternative standard gas instead of He, and this simple NKP method is effective for pore-size evaluation when the difference in the activation energies of permeating gas is small.

3. For the HEDS-derived silica membrane, multiple theoretical lines were obtained when fitting $f_{NKP}^{1/3}$ and $k_{0,i}^{1/3}$ with the gas kinetic diameter with and without SF_6. Without fitting the experimental data of SF_6, the pore sizes of the HEDS-derived silica membrane were calculated to be 0.492 and 0.480 nm from the $f_{NKP}^{1/3}$ plot using He and H_2 as the standard gas, respectively, and to be 0.459 nm from the $k_{0,i}^{1/3}$ plot, which were all smaller than the pore size fitted with SF_6. This result indicates that the membrane had a mass number of pores of approximately 0.459 nm, and a few pinholes that were larger than SF_6 (0.55 nm).

4. For CO_2/CH_4 and O_2/N_2 separations, when the microporous membrane had a uniform pore size that was larger than the kinetic diameters of both gases in the binary system, the ideal selectivities of the membrane decreased significantly as the pore size increased. The predicted and experimental membrane selectivities were in reasonable accordance for various types of microporous membranes.

5. Gas transport behaviors through microporous membranes were significantly affected by the presence of nanosized defects in the membrane. The ideal selectivity for gas separation was decreased with increases in the defect concentration in the membranes, which was much more remarkable for a membrane with a smaller original pore size.

6. For silica membranes with a pore-size distribution, the large pores in the membrane easily affected the gas permeation performance, even when the number of larger pores was small. A small number of large pores generally led to an obvious increase in permeance for relatively large gas molecules, but the increase was unremarkable for small gases.

Notation

a = structural constant given by Eq. 11, m^{-3}
A_0 = physical cross-sectional area of a pore, m^2
A_i = effective cross-sectional area of a pore for the i-th component, m^2
A_m = membrane area, m^2
$d_{e,i}$ = effective diffusion length of the i-th component, m
$d_{k,i}$ = kinetic diameter of the i-th component, m
$d_{k,s}$ = kinetic diameter of the standard gas, m
d_p = pore diameter, m
$d_{p,m}$ = pores diameter of the m-th type of pores, m
$d_{p,mean}$ = mean pore size of the membrane, m
$E_{p,i}$ = activation energy of permeation for the i-th component, kJ mol^{-1}
$E_{pm,i}$ = activation energy of permeation for the i-th component through the m-th type of pores, kJ mol^{-1}
f_m = number-based pore fraction for the m-th type of pores
f_{NKP} = normalized Knudsen-based permeance, dimensionless
$k_{0,i}$ = permeation constant for the i-th component given by Eq. 10, dimensionless
L = membrane thickness, m
M_i = molecular weight of i-th component, kg mol^{-1}
M_s = molecular weight of a standard gas, kg mol^{-1}
N_p = number of pores, dimensionless
$N_{p,m}$ = number of the m-th type of pores, dimensionless
$P_{GT,i}$ = gas-translation model-based permeance for the i-th component, mol m^{-2} pa^{-1} s^{-1}
P_i = permeance for the i-th component, mol m^{-2} pa^{-1} s^{-1}

$P_{K,i}$ = Knudsen diffusion model-based permeance for the i-th component, mol m^{-2} pa^{-1} s^{-1}
$P_{m\text{-}GT,i}$ = modified gas-translation model-based permeance for the i-th component, mol m^{-2} pa^{-1} s^{-1}
P_s = permeance for standard gas, mol m^{-2} pa^{-1} s^{-1}
R = gas constant, J mol^{-1} k^{-1}
T = absolute temperature, k

Greek letters

$\alpha_{i/j}$ = ideal selectivity of the i-th to j-th component, dimensionless
ρ = probability of diffusion for the i-th component, dimensionless
$\rho_{g,i}$ = geometrical probability for the i-th component, dimensionless
ε = porosity, dimensionless
τ = tortuosity, dimensionless

Subscripts

bi = membrane with a bimodal pore-size distribution
mono = membrane with a monomodal pore-size distribution
multi = membrane with a multimodal pore-size distribution

Literature Cited

1. Cao GZ, Meijernik J, Brinkman HW, Burggraaf AJ. Permporometry study on the size distribution of active pores in porous ceramic membranes. *J Membr Sci*. 1993;83:221–235.
2. Tsuru T, Hino T, Yoshioka T, Asaeda M. Permporometry characterization of microporous membranes. *J Membr Sci*. 2001;186:257–265.
3. Hedlund J, Korelskiy D, Sandström L, Lindmark J. Permporometry analysis of zeolite membranes. *J Membr Sci*. 2009;345:276–287.
4. Yoshioka T, Kanezashi M, Tsuru T. Micropore size estimation on gas separation membranes: a study in experimental and molecular dynamics. *AIChE J*. 2013;59:2179–2194.
5. Lee HR, Kanezashi M, Shimomura Y, Yoshioka T, Tsuru T. Evaluation and fabrication of pore-size-tuned silica membranes with tetraethoxydimethyl disiloxane for gas separation. *AIChE J*. 2011;57:2755–2765.
6. Xiao J, Wei J. Diffusion mechanism of hydrocarbons in zeolites-I. *Theory*. *Chem Eng Sci*. 1992;47:1123–1141.
7. Shelekhin AB, Dixon AG, Ma YH. Theory of gas diffusion and permeation in inorganic molecular-sieve membranes. *AIChE J*. 1995;41:58–67.
8. Li G, Kanezashi M, Tsuru T. Preparation of organic–inorganic hybrid silica membranes using organoalkoxysilanes: the effect of pendant groups. *J Membr Sci*. 2011;379:287–295.
9. Kanezashi M, Kawano M, Yoshioka T, Tsuru T. Organic–inorganic hybrid silica membranes with controlled silica network size for propylene/propane separation. *Ind Eng Chem Res*. 2012;51:944–953.
10. Oyama ST, Yamada M, Sugawara T, Takagaki A, Kikuchi R. Review on mechanisms of gas permeation through inorganic membranes. *J Jpn Petrol Inst*. 2011;54:298–309.
11. Yoshioka T, Nakanishi E, Tsuru T, Asaeda M. Experimental studies of gas permeation through microporous silica membranes. *AIChE J*. 2001;47:2052–2063.
12. Lee HR, Shibata T, Kanezashi M, Mizumo T, Ohshita J, Tsuru T. Pore-size-controlled silica membrane with disiloxane alkoxides for gas separation. *J Membr Sci*. 2011;383:152–158.
13. Kanezashi M, Yada K, Yoshioka T, Tsuru T. Design of silica networks for development of highly permeable hydrogen separation membranes with hydrothermal stability. *J Am Chem Soc*. 2009;131:414–415.
14. Nagasawa H, Niimi T, Kanezashi M, Yoshioka T, Tsuru T. Modified gas-translation model for prediction of gas permeation through microporous organosilica membranes. *AIChE J*. 2014;60:4199–4210.
15. Venna SR, Carreon MA. Amino-functionalized SAPO-34 membranes for CO_2/CH_4 and CO_2/N_2 separation. *Langmuir*. 2011;27:2888–2894.
16. Yin H, Wang J, Xie Z, Yang J, Bai J, Lu J, Zhang Y, Yin D, Lin JYS. A highly permeable and selective amino-functionalized MOF CAU-1 membrane for CO_2-N_2 separation. *Chem Commun*. 2014;50:3699–3701.
17. Aoki K, Kusakabe K, Morooka S. Separation of gases with an A-type zeolite membrane. *Ind Eng Chem Res*. 2000;39:2245–2251.
18. Aoki K, Kusakabe K, Morooka S. Gas permeation properties of A-type zeolite membrane formed on porous substrate by hydrothermal synthesis. *J Membr Sci*. 1998;141:197–205.
19. Lovallo MC, Gouzinis A, Tsapatsis M. Synthesis and characterization of oriented MFI membranes prepared by secondary growth. *AIChE J*. 1998;44:1903–1913.
20. Takata Y, Tsuru T, Yoshioka T, Asaeda M. Gas permeation properties of MFI zeolite membranes prepared by the secondary growth of colloidal silicalite and application to the methylation of toluene. *Microporous Mesoporous Mater*. 2002;54:257–268.
21. Tang Z, Dong J. Internal surface modification of MFI-type zeolite membranes for high selectivity and high flux for hydrogen. *Langmuir*. 2009;25:4848–4852.
22. Kusakabe K, Kuroda T, Uchino K, Hasegawa Y, Morooka S. Gas permeation properties of ion-exchanged faujasite-type zeolite membranes. *AIChE J*. 1999;45:1220–1226.
23. Weh K, Noack M, Sieber I, Caro J. Permeation of single gases and gas mixtures through faujasite-type molecular sieve membranes. *Microporous Mesoporous Mater*. 2002;54:27–36.
24. Himeno S, Tomita T, Suzuki K, Nakayama K, Yajima K, Yoshida S. Synthesis and permeation properties of a DDR-type zeolite membrane for separation of CO_2/CH_4 gaseous mixtures. *Ind Eng Chem Res*. 2007;46:6989–6997.
25. Tomita T, Nakayama K, Sakai H. Gas separation characteristics of DDR type zeolite membrane. *Microporous Mesoporous Mater*. 2004;68:71–75.
26. Poshusta JC, Tuan VA, Falconer JL, Nobel RD. Synthesis and permeation properties of SAPO-34 tubular membranes. *Ind Eng Chem Res*. 1998;37:3924–3929.
27. Hong M, Falconer JL, Nobel RD. Modification of zeolite membranes for H_2 separation by catalytic cracking of methyldiethoxysilane. *Ind Eng Chem Res*. 2005;44:4035–4041.
28. Kanezashi M, Shazwani WN, Yoshioka T, Tsuru T. Separation of propylene/propane binary mixtures by bis(triethoxysilyl)methane (BTESM)-derived silica membranes fabricated at different calcination temperatures. *J Membr Sci*. 2012;415–416:478–485.
29. Xu X, Bao Y, Song C, Yang W, Liu J, Lin L. Synthesis, characterization and single gas permeation properties of NaA zeolite membrane. *J Membr Sci*. 2005;249:51–64.
30. Chang K-S, Yoshioka T, Kanezashi M, Tsuru T, Tung K-L. A molecular dynamics simulation of a homogenous organic-inorganic hybrid silica membrane. *Chem Commun*. 2010;46:9140–9142.

Manuscript received Nov. 1, 2014, and revision received Feb. 17, 2015.